Ocean Engineering 356 (2026) 125220

Contents lists available at ScienceDirect

Ocean Engineering

journal homepage: www.elsevier.com/locate/oceaneng

Research paper

Design and lifetime cost optimization of ship energy systems including weather-driven speed profile variability

Foivos Mylonopoulos [a,*], Andrea Coraddu [a], Henk Polinder [a], Andrea Orlandi [b]

[a] Department of Maritime and Transport Technology, Delft University of Technology, 2628 CD, Delft, the Netherlands
[b] ENEA - Italian National Agency for New Technologies, Energy and Sustainable Economic Development, Italy

ARTICLE INFO

Keywords:
Cost
Sizing
Lifetime
Operation
Safety
Weather

ABSTRACT

This study presents a framework for designing and optimizing ship energy systems including weather-driven speed variability and navigation safety constraints. Navigation risks including resonance, surf-riding, and successive high-wave impacts, are calculated using five years of hourly weather data. Random speed variations (up to ±5%) are applied to a baseline speed profile to capture operational uncertainty, and safety-based speed reductions (up to 40%) are applied when required. Course changes are excluded. Treating navigation risks as constraints, operating profiles are generated for different weather conditions. For a conceptually retrofitted cargo ship, hydrogen fuel cell and battery capacities, and their power distribution, are optimized for each operating profile to minimize lifetime energy system cost and assess the effects of weather-induced power variation. Results show that speed and weather variability can significantly change power demand, requiring fuel cell capacities between 700 and 1500 kW. The most common configuration is a 1200 kW fuel cell system with 180 kWh of battery capacity, covering 39% of laden profiles, while full power coverage requires 1500 kW. Lifetime cost outcomes exhibit a 5th–95th percentile spread of −10.3% to +11.1% relative to mean cost. The results demonstrate the significant influence of weather variability on system sizing and cost.

1. Introduction

Shipping facilitates approximately 90% of global trade (Khan et al., 2021). Despite its vital economic role, the sector is responsible for about 10% of the global NO_x emissions and 3% of CO_2 emissions (Gritsenko, 2017). Without effective mitigation measures, this percentage may increase substantially (IMO, 2023). To meet the stringent regulations imposed by regulatory bodies, there is an urgent need for more energy-efficient and environmentally sustainable ships. Enhancing hydrodynamic performance, particularly through sailing speed optimization, remains a key strategy for reducing fuel consumption in both newbuilt and retrofit ships. Moreover, there is growing interest for alternative 'green' fuels such as hydrogen, as substitute for diesel, to lower the lifecycle emissions and ensure regulatory compliance (Balcombe et al., 2019).

Ship fuel efficiency and operational performance are highly sensitive to external disturbances which introduce uncertainty into the vessel's speed and power profiles (Esmailian et al., 2022). If neglected, these variations in operating conditions can lead to suboptimal designs and under or over-estimation of lifetime costs, ultimately affecting economic feasibility.

Several studies have explored the impact of operational uncertainty on ship performance. Esmailian et al. (2022) addressed both weather-related and epistemic uncertainty, during the design stage, optimizing hull and propeller parameters for realistic sea conditions. Lang and Mao (2021) presented a semi-empirical model to predict ship's speed loss at arbitrary wave headings, improving accuracy for voyage optimization. The model estimates added resistance in irregular seas by extending validated formulae originally developed for head regular wave conditions (ISO, 2015). Seo and Oh (2021) analyzed short-term variability in speed–power performance using sea trial data and Monte Carlo simulations, identifying shaft power measurement uncertainty as the dominant factor. Coraddu et al. (2014) modelled speed and displacement as stochastic variables over long-term operational data to evaluate energy efficiency operational indicators via Monte Carlo analysis. Similarly, Fan et al. (2020) developed a Monte Carlo-based energy efficiency model that incorporates environmental parameters (wind, waves, current, water depth), cargo loading, and speed. While the above studies focus on performance prediction or operational assessment under uncertainty, the present work extends this line of research

* Corresponding author.
E-mail address: F.P.Mylonopoulos@tudelft.nl (F. Mylonopoulos).

https://doi.org/10.1016/j.oceaneng.2026.125220
Received 26 November 2025; Received in revised form 9 March 2026; Accepted 21 March 2026

by incorporating weather-driven speed variability into the energy system design optimization of a hydrogen-fuelled ship.

In recent years, various operational strategies have been adopted to reduce fuel consumption and emissions in the maritime sector. Among these, slow steaming, the intentional reduction of sailing speed, has received considerable attention for its potential to significantly improve fuel efficiency, albeit at the cost of reduced voyage frequency and potential revenue loss (Farkas et al., 2022). Numerous studies have highlighted the potential economic and environmental benefits of this approach, which are highly dependent on vessel type, size, trade routes, charter rates, and fuel prices (Degiuli et al., 2021, 2024; Farkas et al., 2022; Pelić et al., 2023). Additionally, weather routing has become a widely adopted operational strategy for optimizing both fuel efficiency and voyage safety by adjusting the ship's route and speed based on forecasted environmental conditions. Zis et al. (2020) presented a survey of ship weather-routing, categorizing existing methods and their application areas. Kytariolou and Themelis (2022) developed a routing optimization tool that incorporates forecasted weather data and seakeeping constraints, enabling both fuel-efficient and safe passage planning. Fabbri and Vicen-Bueno (2019) highlighted the importance of navigational risk assessment, while De Gracia et al. (2018) demonstrated how weather-informed routing can reduce fatigue damage and protect hull integrity under varying sea states. Pennino et al. (2020) used a Dijkstra-based routing model to enhance seakeeping performance with minimal impact on voyage duration. While these studies clearly demonstrate the advantages of slow steaming for fuel efficiency and weather routing for enhancing safety under environmental uncertainty, there is limited literature exploring speed adjustments as a proactive safety measure, rather than solely to reduce fuel consumption or emissions.

The previously referenced studies have extensively explored strategies for reducing fuel consumption and emissions through operational adjustments and hydrodynamic performance improvements. In recent years, there has been increasing interest toward alternative fuelled ships, to achieve substantial emission reductions. Hydrogen fuel cells have emerged as a promising zero-emission alternative to conventional diesel propulsion systems, with their adoption seen as vital for regulatory compliance (Mylonopoulos et al., 2024). Several studies have focused on energy system sizing and operation for hydrogen-fuelled ships. Pivetta et al. (2021) and Dall'Armi et al. (2021) conducted multi-objective optimizations accounting for fuel cell and battery degradation, while Dall'Armi et al. (2022) extended this work by incorporating uncertainty in fuel and component costs using Montecarlo simulations. Bassam et al. (2016b) evaluated multiple system configurations to identify the optimal topology in terms of total energy system cost. Other studies focused on developing energy management strategies for control of fuel cell-battery hybrid ship systems to optimize the power distribution for fixed design parameters (Bassam et al., 2016a, 2017; Han et al., 2014; Zhang et al., 2020). However, the previous optimization studies assume static or simplified power profiles without accounting for variability in power demand due to operational uncertainty. This may limit the accuracy of lifetime cost assessments and energy system design and operation. Only a few energy system design and operation optimization studies have introduced some degree of operational variability. Vieira et al. (2022) evaluated two uniform-demand scenarios by scaling the baseline power profile by $\pm 10\%$ across all timesteps: one profile fixed at $+10\%$ and another fixed at -10%, and Wang et al. (2021) used four pre-defined power profiles based on historical vessel data for a nested design and control optimization. Both studies perform multi-objective optimizations, for diesel-fuel cell-battery hybrid systems, in terms of costs and emissions, and consider only a few fixed power profiles to represent how the vessel operates, which means they may not capture the full variability that occurs under real weather and sea conditions. The present work extends this line of research by introducing weather-driven speed variability based on 5 years of weather data, and by incorporating navigation risk-based speed constraints into a lifetime cost minimization framework.

To the best of the authors' knowledge, no study to date addresses lifetime cost optimization for vessel propulsion systems under operational uncertainty and weather-induced speed profile variability. This research addresses this gap by focusing on the design and lifetime operation of hydrogen-based ship energy systems.

The key contributions of this work are highlighted below.

- Development of a holistic framework that jointly optimizes energy system sizing and operation by integrating weather-driven speed profile variability into a lifetime cost minimization problem.
- Incorporation of safety-driven speed adjustments as a proactive operational strategy for reducing navigation risks under adverse weather conditions.

The remainder of this paper is organized as follows: Section 2 outlines the specifications and operational characteristics of the case vessel. Section 3 describes the proposed methodology for the lifetime cost optimization, including speed profile variability. Section 4 discusses the key results from the optimization analysis. Finally, Section 5 draws conclusions and offers recommendations for future research.

2. Case study

The case vessel in this study is a 90-m-long, 12.5-m-wide general cargo ship with an approximate deadweight of 3700 tons (Mylonopoulos et al., 2024). It is assumed to operate along a fixed route in the Baltic Sea between Sweden and Lithuania, completing 80 laden and 80 ballast voyages annually, each lasting around 29 h (depending on the speed). This repeated voyage enables an investigation into how variability in speed and power demand, due to different weather conditions, affects the lifetime cost. A baseline speed profile (Fig. 1), and the course over ground of the vessel as a function of time, derived from historical onboard measurement data, are used as input to the analysis. To reduce the ship's environmental footprint, its original diesel engine propulsion system is conceptually replaced by a proton exchange hydrogen fuel cell system, supported by lithium-ion batteries (Mylonopoulos et al., 2024). The vessel is assumed to have a remaining operational lifetime of 20 years after retrofitting.

3. Methodology

The proposed methodology, illustrated in Fig. 2 consists of two main steps.

- Step 1: Data collection and analysis.

Historical weather and ship operational data are gathered. ERA5 hourly wind and wave data (Copernicus Climate Change Service, 2018),

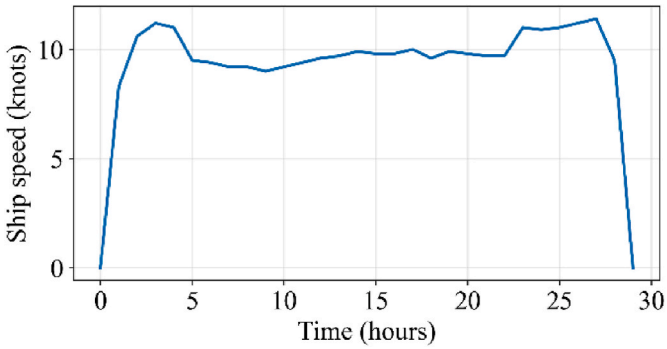

Fig. 1. Baseline speed profile of the case ship (17-18 March 2022).

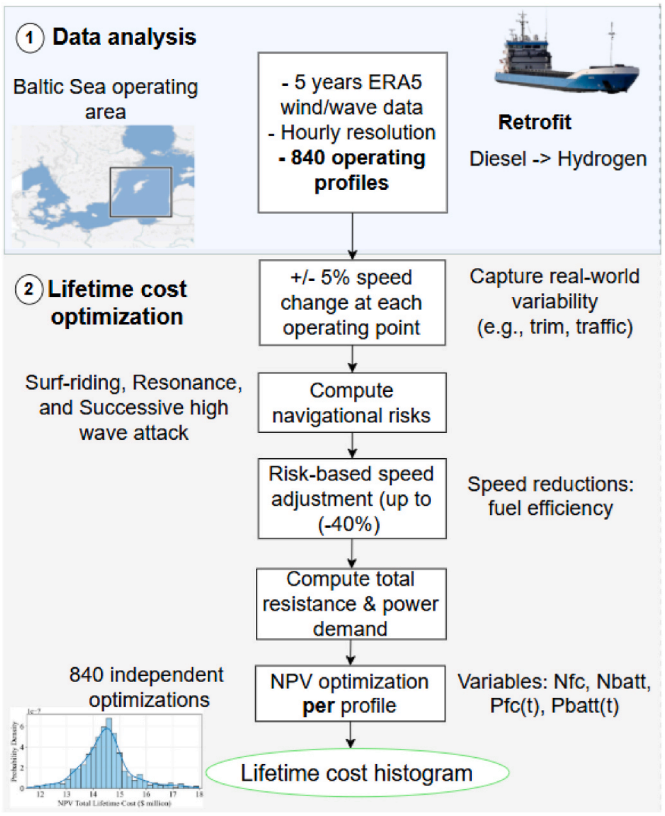

Fig. 2. Methodology diagram.

along with onboard measurements of ship speed and heading, are used as input to calculate relative wind and wave directions.

- Step 2: Lifetime cost optimization.

Operating profiles are created by starting from the original ship speed profile, then applying a±5% random speed variation (at each time step) to reflect operational uncertainty, and then applying the necessary adjustments to ship speed driven by weather conditions to mitigate navigation risks (surf-riding, resonance and successive high-wave impacts). Ship resistance and power demand are then calculated based on the resulting speed profiles.

An optimization framework is developed to quantify the impact of speed and power-profile variability on lifetime cost of the ship energy system. The framework optimizes total fuel-cell and battery capacities, and their time-varying power outputs, to minimize the Net Present Value (NPV) of total lifetime cost for each operating profile. The selected design configuration must cover all the power profiles (including extreme power-demand scenarios). Model outputs include the optimal design parameters and the lifetime cost distribution.

3.1. Data collection and analysis

To capture seasonal and interannual weather variability, while maintaining computational efficiency, operating periods from all days of each month over the last five years are selected, resulting in a broad representation of realistic operating conditions across multiple seasons and years. The objective of the study is energy system sizing and lifetime cost assessment under realistic operating conditions, rather than maneuvering performance or vessel response to short-duration transient power spikes. Given the largely steady operating profile of the case vessel (Mylonopoulos et al., 2024), the adopted hourly temporal resolution is considered appropriate for the present techno-economic scope. High temporal resolution environmental data are typically available only from in-situ measurements, which usually cover limited spatial areas and short time periods, and therefore do not provide the multi-year spatial coverage required for the present analysis. Sub-hourly environmental fluctuations are not expected to change optimal system capacities within the lifetime cost-driven system sizing framework developed in this study.

The wind speed, wind direction, significant height of combined wind waves and swell, mean wave direction, and wave period are extracted from the ERA5 dataset to generate load profiles for different weather conditions along the vessel's operational route (Copernicus Climate Change Service, 2018; ISO, 2015).

A total of 840 operating profiles are generated (14 profiles per month over 5 years, each lasting approximately 29 h depending on ship speed), each corresponding to a distinct set of historical hourly wind and wave conditions extracted from ERA5 (Copernicus Climate Change Service, 2018). Each profile represents one deterministic weather-based operating case. For a given case (profile), the vessel is assumed to perform 80 round trips per year (80 laden voyages and 80 ballast return voyages) over its 20-year remaining lifetime under the same environmental conditions represented by that profile. The ballast leg is included by reversing the vessel heading while maintaining the same hourly environmental conditions and baseline speed profile. This ensures that the lifetime cost calculation reflects complete round trips (laden and ballast) for each weather case. Considering both laden and ballast loading conditions reflects realistic commercial vessel operation and avoids bias in lifetime cost estimation that would arise from modelling only a single loading condition or a single sailing direction.

The 840 profiles are not assumed to occur within the same operational year. Instead, each profile is analyzed independently to evaluate how different realistic weather conditions affect optimal system sizing and lifetime cost. The optimization is performed independently for each of the 840 weather-based power profiles. This allows the assessment of how different realistic environmental and operating conditions influence optimal system sizing and lifetime cost. In contrast to approaches that assume a single power profile repeated over the lifetime (Bassam et al., 2016b; Dall'Armi et al., 2021), the present study quantifies the variability of optimal designs and cost outcomes across a wide range of historical operating conditions. The final selected configuration is chosen to ensure full power coverage across all profiles, incorporating a practical capacity margin for operational robustness.

The wave period, wave height, ship's speed, and relative wave direction, are critical parameters for assessing navigational risks (IMO, 2007).

3.2. Optimization framework

3.2.1. Generation of speed and power demand profiles

Weather variability is represented through five years of historical ERA5 wind and wave data, from which 840 distinct hourly weather-based operating profiles are constructed. These profiles capture realistic environmental variability across a wide range of operating conditions from multiple seasons and years. Within each profile, the environmental conditions are treated as deterministic, as each profile represents one specific historical weather-based operating case. The objective of this modelling approach is to capture realistic weather-driven operational variability rather than to perform full probabilistic metocean uncertainty propagation. In addition to weather effects, a random speed variation of up to ±5% is applied at each time step to represent operational variability unrelated to environmental conditions, such as trim changes, machinery control deviations, pilotage decisions, and traffic effects, based on discussions with the vessel operators. The selected bound is intended to represent modest operational variability while keeping the resulting profiles close to the baseline speed profile.

For each speed profile, after applying the random speed changes, the associated navigation risks, including surf-riding, resonance, and

successive high wave attacks, are calculated and assessed to ensure safe and realistic operating conditions.

Surf-riding typically occurs when a vessel sails in following or stern quartering seas (waves approaching from astern) and is situated on the forefront of a steep wave. This can lead to rapid accelerations and potentially trigger the broaching-to phenomenon, where the ship experiences an uncontrollable yawing motion and large heeling angles, increasing the risk of capsizing. According to the guidelines provided by the International Maritime Organization (IMO) (IMO, 2007), surf-riding risks are particularly high within the following conditions, shown in Equations (1) and (2):

$$1.8 \leq \frac{V_s}{\sqrt{L}} \leq 3 \tag{1}$$

and

$$135 \leq \alpha \leq 225\ (^\circ) \tag{2}$$

where.

- V_s is the ship speed (knots)
- $L = 90$ m. is the ship's length
- α is the relative wave direction (degrees)

Resonance refers to the amplification of ship motions when the wave encounter period (T_E) is almost equal to the ship's natural roll period (T_N) or half of it. The two periods are defined as shown in Equations (3) and (4) based on (IMO, 2007; Papanikolaou, 2014).

$$T_E(t) = \frac{3 \cdot T_w^2(t)}{3 \cdot T_w(t) + V_s(t) \cdot \cos(\alpha)}\ (\mathrm{s}) \tag{3}$$

$$T_N = \frac{2 \cdot \pi \cdot 0.38 \cdot B}{\sqrt{g \cdot GM}}\ (\mathrm{s}) \tag{4}$$

where.

- t is the time (seconds)
- T_w is the wave period (seconds)
- $B = 12.5$ m is the ship's breadth
- $g = 9.81$ m/s^2 is the gravitational acceleration
- GM is the transverse metacentric height: 0.36 m in laden condition and 1.74 m in ballast condition (Mylonopoulos et al., 2026).

To mitigate resonance-related risks, such as synchronous rolling (Equation (5)) and parametric rolling (Equation (6)), the following criteria are applied (Krata and Wawrzyński, 2016):

$$|\, T_E(t) - T_N| > 1\ (\mathrm{s}) \tag{5}$$

$$|\, T_E(t) - 0.5 \cdot T_N| > 1\ (\mathrm{s}) \tag{6}$$

These constraints ensure that the wave encounter period does not closely match the ship's natural period or half of it, thus reducing the likelihood of resonance.

According to (IMO, 2007), successive wave attack risks can be present, at following or stern quartering seas, for the operating conditions shown in Equations (7) and (8):

$$1.6 \leq \frac{V_s}{T_w} \leq 2.4 \tag{7}$$

and

$$140 \leq \alpha \leq 220, (^\circ) \tag{8}$$

The successive wave attack risks are particularly high for significant wave heights $h_s > 0.04 \cdot L$ (IMO, 2007).

To mitigate the risks of surf-riding, resonance, and successive high-wave attacks, the ship's speed is adjusted while assuming a fixed course throughout the voyages. Course changes are out of scope for this study, as the focus is on evaluating speed-based risk mitigation and its impact on energy system and lifetime cost. Discussions with vessel operators indicated that engine power reduction, and thus speed adjustment, is their primary risk-mitigation strategy. Based on these discussions, the minimum required speed adjustment is applied when necessary, within operational bounds, limited to a maximum reduction of 40%, which was identified by the vessel operators as the practical limit in real operation. Such speed reductions can enhance safety, improve fuel efficiency, and limit peak power demand and energy system size. Speed increases were not considered as a mitigation strategy, as increasing engine power to avoid resonance condition would lead to higher fuel consumption and is not commonly applied in practice according to vessel operators. The resulting safety-adjusted speeds are then used to determine the voyage duration for the fixed sailing distance, which in turn affects the fuel consumption per trip.

For each scenario, the updated speed profiles are used to estimate the total ship resistance (R_t), as shown in Equation (9):

$$R_t = R_{calm} + R_{wave} + R_{wind} \tag{9}$$

where.

- R_{calm} is the calm water resistance (N), derived from the resistance-speed curves of the case ship for both laden and ballast conditions. The resistance-speed curves (provided by the vessel operators) are shown in Fig. 3. Within the available speed range, resistance values are obtained by linear interpolation of the provided data. Outside this range, linear extrapolation is applied to ensure continuity of the power demand curve. The extrapolated low-speed values have a negligible impact on optimal system sizing and lifetime cost.
- R_{wave} is the added wave resistance (N)
- R_{wind} is the added wind resistance (N)

The added wind resistance is calculated using Equation (10), based on (ITTC, 2005):

$$R_{wind} = 0.5 \cdot \rho_A \cdot A_{XV} \cdot C_{AA}(\psi_{WR}) \cdot V_{WR}^2 \tag{10}$$

where.

- $\rho_A = 1.225$ kg/m^3 is the air density
- A_{XV} (m^2) is the vessel's transverse projected area to the wind: 117.2 m^2 in the laden condition and 143.1 m^2 in ballast. The higher value

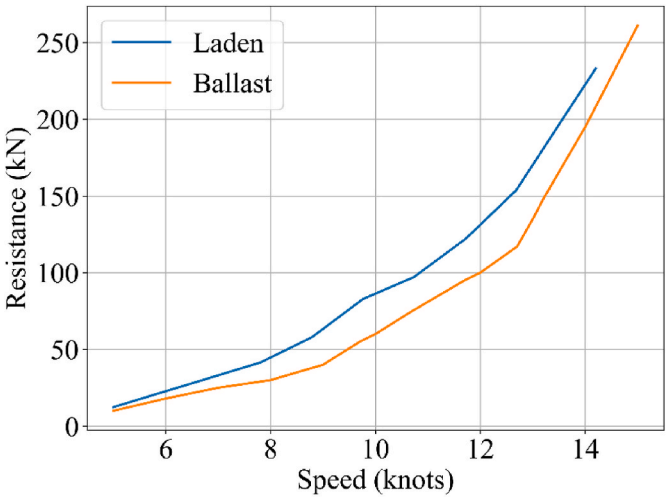

Fig. 3. Resistance-speed curves for laden and ballast conditions.

in the ballast condition reflects the reduced draft, which increases the above-water area exposed to wind.

- $C_{AA}(\psi_{WR})$ is the wind resistance coefficient as a function of the relative wind direction, derived from (ISO, 2015).
- V_{WR} (m/s) is the relative wind velocity, computed using Equation (11), based on (Aijjou et al., 2020).

$$V_{WR} = \sqrt{V_{s\_ms}^2 + V_{TW}^2 + 2 \cdot V_{s\_ms} \cdot V_{TW} \cdot \cos(\alpha)} \tag{11}$$

where.

- $V_{s\_ms} = 0.5144 \cdot V_s$ is the ship speed converted from knots to m/s
- V_{TW} (m/s) is the true wind speed from ERA5.

The maximum added wave resistance (X_d), over relative wave directions from head to 30° off-bow, can be calculated using Equation (12), based on (IMO, 2021).

$$X_d = 1336 \cdot (5.3 + V_{s\_ms}) \cdot \left(\frac{B \cdot d}{L}\right)^{0.75} \cdot h_s^2 \tag{12}$$

where.

- d is the ship's mean draft: 5.3 m in laden condition and 3.23 m in ballast condition.

The added wave resistance for any relative wave direction can be approximated using Equation (13), based on (IMO, 2021; Lang and Mao, 2021):

$$R_{wave} = \begin{cases} X_d \cdot \cos^2(\alpha), \alpha \in [0, 90] \cup [270, 360] \\ 0, otherwise \end{cases} \tag{13}$$

This approach aligns with other studies that have assumed zero added wave resistance in following and stern quartering seas (ISO, 2015; Mittendorf et al., 2022) noting that the degree of uncertainty in estimating this component often exceeds its actual magnitude. The widely adopted STA-1 and STA-2 methods assign zero added resistance for relative wave directions between 90° and 270° (Esmailian et al., 2022; ITTC, 2005). Hence, in following and stern-quartering seas (90° - 270°), the added wave resistance is approximated as zero. In these conditions, the added resistance is generally small and may even become negative due to wave-assisted propulsion effects. Therefore, using a zero approximation provides a reasonable first-order representation for the purpose of this study, which focuses on energy system sizing and lifetime cost assessment rather than detailed hydrodynamic modelling, which would increase modelling and computational complexity. In addition, peak power demand in the dataset is mainly driven by head and bow-quartering sea states, which can be calculated using the IMO-provided formulation (Equation (12)). While recent research has introduced more advanced semi-empirical models for added wave resistance (Kim et al., 2022; Mittendorf et al., 2022; Park et al., 2019), incorporating such detailed models lies beyond the scope of this study.

The required propulsive power demand (P_{demand}) in kW, is then calculated using Equation (14), based on (Esmailian et al., 2022):

$$P_{demand} = \frac{R_t \cdot V_{s\_ms}}{1000 \cdot n_t} \tag{14}$$

where.

- n_t is the total propulsive efficiency. The values are provided, by the vessel operators, as a function of ship speed for both laden and ballast conditions, and are summarized in Table 1. Within the available speed range, propulsive efficiency values are obtained by linear interpolation of the provided data. Outside this range, linear extrapolation is applied to ensure continuity of the power demand curve. The extrapolated low-speed values have a negligible impact on optimal system sizing and lifetime cost.

Table 1
Propulsive efficiency values as a function of speed for laden and ballast conditions.

Ship speed (knots)	$n_{t-laden}$	$n_{t-ballast}$
5	0.631	0.736
6	0.629	0.735
7	0.624	0.733
8	0.618	0.729
9	0.609	0.723
10	0.598	0.714
11	0.601	0.704
12	0.595	0.698
13	0.585	0.689
14	0.565	0.668

The resistance-based propulsion power estimation (Equation (14)) captures the dominant hydrodynamic contributions (calm-water resistance, added wind and wave resistance) relevant for system-level techno-economic analysis. However, it does not aim to reproduce exact historical shaft power measurements, which are influenced by additional in-service factors such as hull fouling, machinery condition, operational scheduling decisions, and traffic constraints. Therefore, the present framework is intended for energy system sizing and lifetime cost assessment under various weather-driven scenarios rather than time-series replication of specific historical voyages.

3.2.2. Total cost optimization

The goal of the optimization is to determine the optimal system capacities and power distribution between fuel cells and batteries, for each power profile, that minimize the NPV, under operational uncertainty and weather-driven speed profile variability.

The fuel consumption as a function of time is calculated using the quadratic expression shown in Equation (15):

$$F_{FC}(k) = a \cdot P_{FC}^2(k) + b \cdot P_{FC}(k) + c \tag{15}$$

where.

- k represents the discrete time steps ($k = 0,1,2 \ldots K$)
- $P_{FC}(k)$ is the fuel cell power output in kW, at time step k (control variable).
- $a = 0.0066, b = 1.4025, c = 1.8306$ are the coefficients derived from the fuel cell efficiency curve, provided by the manufacturer (PowerCell Sweden AB, 2019). The fuel cell stack is rated at 100 kW. Fig. 4 shows the characteristic curve of the fuel cell, with fuel consumption (expressed in kW) on the y axis, and output power (kW) on the x axis (Pivetta et al., 2021). The F_{FC} (kW) is derived from the ratio of output power over efficiency.

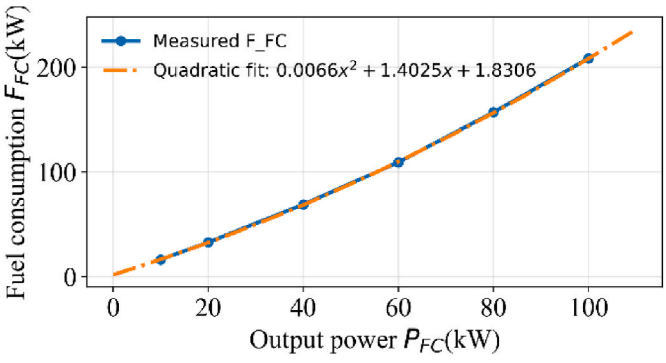

Fig. 4. Fuel consumption curve.

The total fuel consumption for a single voyage, accounting for all fuel cells, is computed in kilograms using Equation (16):

$$F_{total} = N_{FC} \sum_{k=0}^{K} (\mathrm{F}_{FC}(k) \cdot \Delta t \cdot c_{e-m}) \tag{16}$$

where.

- K is the total number of time steps in a voyage profile.
- N_{FC} is the number of 100-kW fuel cells (design variable).
- Δt is the time step duration. Its value is 1 h, aligned with the temporal resolution of the ERA5 environmental data used in this study. This 1-hr time step is consistent with practices commonly adopted in the literature for weather-driven ship performance assessment studies (Fabbri and Vicen-Bueno, 2019; Lang and Mao, 2021), but also for energy system design-operation analysis (Liu et al., 2019; Vahabzad et al., 2022; Zhang et al., 2025).
- c_{e-m} = 0.03 kg/kWh is the energy-to-mass conversion coefficient (Banaei et al., 2021).

The battery State of Charge (SoC) as a function of time is expressed based on (Wang et al., 2021), as shown in Equation (17):

$$SoC_{batt}(k) = SoC_{batt}(k-1) - \frac{P_{batt}(k) \cdot \Delta t}{E_{batt,rated}} \tag{17}$$

where.

- $P_{batt}(k)$ is battery power output in kW, at time step k (control variable). Positive power values indicate discharging.
- $E_{batt,rated}$ = 60 kWh is the rated energy capacity of the battery, based on the manufacturer data (Praxis Automation Technology B.V., 2024).

To limit degradation, the battery C-rate is constrained between −1 and 1, and the SoC is bound between 20 and 80% (Praxis Automation Technology B.V., 2024). The initial and final SoC are set to 50% for energy balance without requiring shore charging.

The constraint for the power balance at each time step is shown in Equation (18), ensuring that the combined output from fuel cells and batteries matches the power demand, considering the efficiencies of the powertrain components.

$$N_{FC} \cdot P_{FC}(k) + N_{batt} \cdot P_{batt}(k) = \frac{P_{demand}(k)}{n_{conv} \cdot n_{inv} \cdot n_{motor} \cdot n_{gb}} \tag{18}$$

where.

- N_{batt} is the number of 60-kWh batteries (design variable). The installed battery capacity should be at least 180 kWh for emergency conditions (Mylonopoulos et al., 2024).
- $P_{demand}(k)$ is the required propulsive power demand at time step k, obtained from Equation (14).
- n_{conv}, n_{inv}, n_{motor}, n_{gb} are the efficiencies of converters, inverter, motor, gearbox for the new powertrain, taken as: 0.985, 0.985, 0.96, and 0.98 respectively, based on literature and manufacturer-based values as documented in the authors' previous study (Mylonopoulos et al., 2026).

This power balance equation is a mixed integer nonlinear constraint due to the product of integer design variables and continuous control variables.

The objective of the optimization problem is to minimize the total lifetime cost, which includes the initial capital expenditure (CAPEX) and the NPV of operational expenditure (OPEX), as expressed in Equation (19):

$$\min_{(N_{FC_i}, N_{batt_i} P_{FC}(t), P_{batt}(t))} (CAPEX_i + NPV_{OPEX,i}) \tag{19}$$

where.

- i denotes each operating profile.

This objective function is a mixed integer nonlinear equation due to the product of integer design variables and continuous control variables.

The initial investment (CAPEX) includes the purchase costs for the fuel cell and battery systems, as shown in Equation (20):

$$CAPEX_i = N_{FC_i} \cdot P_{FC,rated} \cdot C_{FC} + N_{batt_i} \cdot E_{batt,rated} \cdot C_{batt} \tag{20}$$

where.

- $P_{FC,rated}$ = 100 kW is the rated fuel cell power.
- C_{FC} = 1014 $/kW is the cost per kW for the fuel cell stack (Mylonopoulos et al., 2024).
- C_{batt} = 492 $/kWh is the cost per kWh for the battery (Mylonopoulos et al., 2024).

The NPV of OPEX includes both the discounted fuel costs and component replacement costs and is calculated as shown in Equation (21):

$$NPV_{OPEX,i} = NPV_{replace,i} + NPV_{fuel,i} \tag{21}$$

The NPV of the replacement costs is calculated as shown in Equation (22):

$$NPV_{replace,i} = \sum_{t=1}^{T} \left(\left(\frac{b_{FC,replace_t} \cdot N_{FC_i} \cdot P_{FC,rated} \cdot C_{FC,replace}}{(1+r)^t} \right) + \left(\frac{b_{batt,replace_t} \cdot N_{batt_i} \cdot E_{batt,rated} \cdot C_{batt,replace}}{(1+r)^t} \right) \right) \tag{22}$$

where.

- t is the time in years, and T = 20 years is the vessel's remaining lifetime.
- $b_{FC,replace_t}$ is a binary variable for fuel cell replacement in year t (approximately every 4 years, based on 20,000 operating hours (PowerCell Sweden AB, 2019)).
- $b_{batt,replace_t}$ is a binary variable for battery replacement in year t (assumed every 7 years (Mylonopoulos et al., 2024)).
- $C_{FC,replace}$ and $C_{batt,replace}$ are the replacement fuel cell and battery costs in $/kW, which are assumed to be 50% of their initial CAPEX, based on the reduced projected prices due to increased market adoption (Mylonopoulos et al., 2024).
- r = 5% is the interest rate (Lagemann et al., 2023; Pericic et al., 2022; Soni et al., 2023).

Fuel cell lifetime is represented using a simplified approach based on manufacturer-provided limits (Mylonopoulos et al., 2026), while battery replacement timing is based on the degradation analysis presented in Mylonopoulos et al. (2024). In the present study, degradation is therefore represented through time-based replacement rather than detailed dynamic aging modelling. This avoids relying on degradation parameters mainly derived from automotive applications, which may not accurately reflect maritime operating conditions and could yield unreliable results (Mylonopoulos et al., 2026). This approach remains consistent with the techno-economic scope of the present framework.

The NPV of the lifetime fuel cost for each profile is calculated as shown in Equation (23):

$$NPV_{fuel,i} = \sum_{t=1}^{T} \frac{F_{total,i} \cdot N_{annual,trips} \cdot C_{h_2}}{(1+r)^t} \quad (23)$$

where.

- $N_{annual,trips}$ is the number of annual trips
- C_{h_2} = 6$/kg is the baseline price of hydrogen fuel, based on (Mylonopoulos et al., 2024). Due to fuel price uncertainty, the impact of different green hydrogen prices (3$/kg and 9$/kg) on the total lifetime cost, will be discussed.

The resulting optimization is a Mixed Integer Nonlinear Programming (MINLP) problem solved with the open-source solver SCIP. SCIP uses various techniques including: presolving, branch-and-bound search, cutting planes, and heuristics to efficiently explore the design space without excessive computational demands (Bestuzheva et al., 2023).

The optimization framework produces a distribution of optimal solutions, with required system capacities and power distribution between fuel cells and batteries for each power profile. The selected design should cover the power profiles of the ship with the minimum NPV.

4. Results

4.1. Data collection and analysis results

The minimum, maximum, and mean values of the wind and wave parameters, obtained from ERA5 data, are summarized in Table 2. Over the past five years, conditions across the vessel's operating area are generally moderate. The mean significant wave height is 1.03 m and the mean wind speed is 6.77 m/s. Higher wind speeds are consistently associated with higher significant wave heights in the dataset, reflecting the physical dependency between the two parameters. Similarly, relative wind and wave directions are generally aligned, with only small deviations across operating points, as expected when local wind drives wave development. About 9% of operating points show angular differences greater than 50 °, likely reflecting swell contributions.

For data validation purposes, wind direction measurements from onboard log data and ERA5 are compared, as shown in Fig. 5. These wind profiles span from 12:00 on March 17, 2022 until 17:00 on the following day. The two datasets exhibit similar overall trends, with minor differences in wind direction observed throughout the baseline voyage. These deviations are primarily attributed to the spatial and temporal resolution differences: ERA5 provides hourly, spatially averaged data over the vessel's operating area, which may not fully capture localized gusts or small-scale phenomena. In contrast, the onboard measurements are recorded at a higher frequency (every 5 min) enabling finer resolution of local conditions. Larger discrepancies are observed at the beginning and end of the voyage, likely due to vessel manoeuvring or stationary periods at port. However, these effects are limited and do not significantly influence the overall trend. Therefore, for the purpose of this study, the accuracy of ERA5 data is deemed sufficient.

4.2. Optimization results

4.2.1. Navigation risk reduction

By applying risk-based speed adjustments, the total risk in the dataset decreases substantially from 25.25% to 6.38% (of total operating points of all profiles), with an average speed reduction of 17.6%. Specifically, the resonance risk is reduced from 13.04% to 4.51% and the successive wave attack risk from 12.21% to 1.88%. Surf-riding and broaching risks are absent throughout, since the velocity-to-length ratios ($V/\sqrt{L}$) remain below the critical threshold of 1.8. This finding is consistent with feedback from the vessel operators, who confirmed that surf riding is not a concern for the case vessel.

A further reduction in risk from 6.38% to 4.28% could, theoretically, be achieved through modest speed increases (up to 10%), by shifting the encounter frequency away from the natural ship frequency at certain relative wave directions that speed reductions (up to 40%) are not effective. However, this option was not recommended by vessel operators, primarily due to its negative impact on fuel efficiency.

Additional sensitivity tests also showed that unrealistically large speed reductions up to 90% would reduce the remaining risk to approximately 1.6%, confirming that most residual cases arise from the imposed practical speed-reduction limit rather than modelling limitations.

The remaining risks (6.38% of operating points) correspond mainly to resonance conditions in near-beam seas ($\alpha \approx 90^\circ$ or 270°), where speed adjustments have limited influence on the wave encounter period (Equation (3)). Based on discussions with the vessel operators, such residual risks may occur in real ship operations but are considered operationally manageable for this vessel, provided they occur under rare conditions and do not coincide with exposure to critical sea states. For the case vessel, these critical conditions correspond to short wave periods of approximately 4-8 s combined with significant wave heights exceeding 4 m. The residual risk cases in the dataset do not coincide with these conditions, so they are considered operationally manageable. Course changes or weather routing could further reduce the remaining risks, but investigating coupled speed-routing strategies lies outside the scope of the present study.

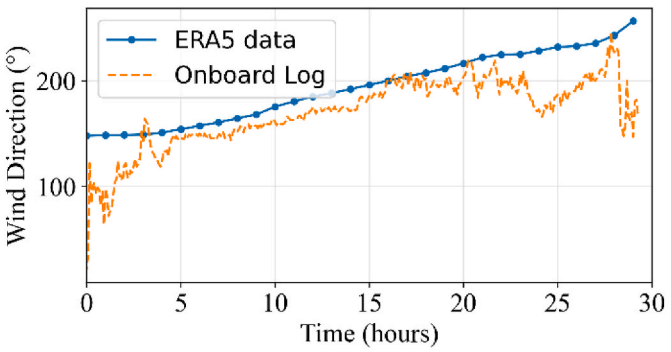

Fig. 5. Wind direction comparison: Onboard log vs ERA5 (baseline profile).

Table 2
ERA5 weather data.

Weather parameter	Min.	Mean	Max.
Wave height (m)	0.13	1.03	4.65
Wave period (s)	2.36	4.95	9.15
Wind speed (m/s)	1.1	6.77	16.7

4.2.2. Weather impact on power profiles and energy system sizing

The sizing analysis focuses on the laden part of the voyage, which represents the scenario with maximum resistance and power demand. The ballast condition involves lower energy demands and does not drive energy system sizing. Once the design configuration is selected based on the most energy-intensive (laden) power profiles, the total lifetime cost is estimated by also including the ballast voyages to account for the total lifetime fuel consumption over full round trips. For the ballast condition, the same baseline speed profile as the laden leg is applied, with a 180° heading change (reverse track), and power demand is recalculated, for each power profile, using ballast-condition parameters.

The vessel's power demand is estimated using the safety-adjusted speeds. The resulting probability distribution of power demand during sailing in laden condition is shown in Fig. 6. The mean power demand is 778 kW. The 90th and 95th percentiles occur at 1181 kW and 1286 kW, respectively. The low-power region corresponds to cases where large

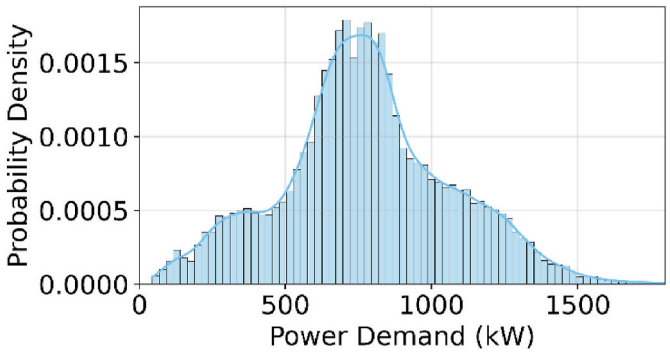

Fig. 6. Histogram of power demand during sailing periods in laden condition.

speed reductions (30–40%) are applied at already low operating speeds (≈8 knots) to mitigate navigation risks.

The distributions of required fuel cell and battery capacities, for all the different operating profiles in laden condition, are shown in Fig. 7. The mean fuel cell capacity is approximately 1200 kW, with 58% of all simulations falling within the 1200-1300 kW range (Fig. 7a). Low fuel cell capacities of 700-900 kW are required in 2.86% of the profiles, primarily due to frequent and substantial speed reductions applied for safe operation. High capacities of 1400-1500 kW are required in 12.5% of the profiles, primarily driven by high added resistance in combination with relatively high speeds (e.g. >10.5 knots) at the specific operating points. These cases usually involve near-head seas, where the safety logic does not trigger speed reductions (no surf-riding, resonance, or successive wave attack risks), so the vessel keeps its speed while facing high resistance.

The battery capacity histogram shows a much more skewed distribution, with a mean of 258 kWh and 83.5% of the cases concentrated in the 180–300 kWh range (Fig. 7b), where the battery is used primarily for peak shaving. Battery capacities exceeding 480 kWh occur only in 5.3% of the profiles, corresponding to rare scenarios with short periods of high peak power or cases with highly fluctuating power demand induced by random speed changes and safety-based speed adjustments. In such scenarios, a larger battery capacity is selected to buffer peaks, maintain

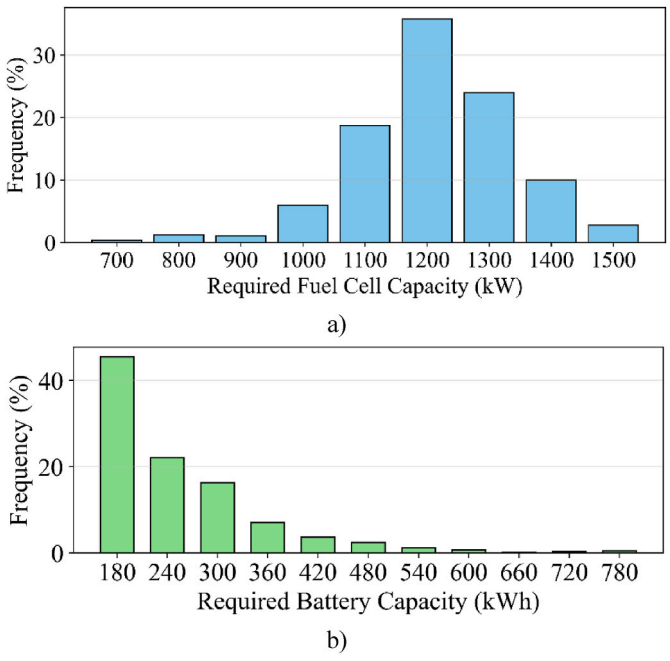

Fig. 7. Histograms of required system capacities: a) Fuel cells, b) Batteries. Frequencies are expressed as percentages of all laden power profiles.

fuel cell efficiency, and satisfy SoC constraints. Overall, because the battery is primarily used for peak shaving and its optimal capacity remains limited across most profiles, the adopted hourly temporal resolution is expected to be sufficient for determining optimal system capacities within the present lifetime cost-driven sizing framework.

The most frequent configuration across all simulations in laden condition, consists of a 12 × 100 kW fuel cell system and a 3x60 kWh battery system, covering 39% of the laden power profiles. The remaining load profiles either require more battery capacity (Fig. 7b) or exhibit sustained peak loads above 1.2 MW which require higher installed fuel cell capacity (Fig. 7a). For full power coverage of all profiles with 1200 kW fuel cell capacity, the ship's speed would need to be reduced. However, this would result in fewer voyages and lower revenue, and for that reason it is not chosen.

Some of the vessel's power profiles, for different weather conditions, are plotted in Fig. 8.

- An average-power operating profile (Fig. 8a), without any navigation risks and speed reductions applied. The optimizer selects 12 × 100 kW fuel cells, 3x60 kWh batteries for this power profile.
- A low-power operating profile (Fig. 8b) that takes longer to be completed (33.9 h) due to frequent and high-speed reductions applied for safe operation. An average speed reduction of 19.9% is applied across 53.3% of the specific profile's operating points to eliminate resonance and successive wave attack risks. The optimizer selects low energy system capacities of 7 × 100 kW fuel cells and 3x60 kWh batteries.
- A high-power operating profile during winter period (Fig. 8c), with high operating speed (>10.5 knots) at near-head seas, (high added resistance without triggering speed reductions) for over 2 h towards the end of the voyage. The optimizer selects 15 × 100 kW fuel cells and 3x60 kWh batteries.
- A power profile experiencing high fluctuations (Fig. 8d). High speed reductions are applied to eliminate risks at two operating points; at ~28hr and 30hr, with high operating speed between those points at 29 h (without risk-based speed reduction), reaching a peak power level of 1275 kW. The optimizer selects 10 × 100 kW fuel cells and 9x60 kWh batteries for this profile, to buffer short-duration high peak.

Based on the above, for full power coverage, the installed fuel cell capacity needs to be 1500 kW. Such design choices align with common practice in the maritime industry, where a 20–25% capacity margin is often used for the main power source to enhance reliability under extreme conditions. Hence, the selected configuration consists of 15 × 100 kW fuel cells, and 3x60 kWh batteries.

The vessel's power demand depends on the combined influence of ship speed and weather conditions (significant wave height, wind speed, relative wind and wave directions). Table 3 presents selected cases under different speeds and weather conditions. To examine the contribution of each factor three pairs of operating points are compared.

1) ship speed varies under similar seas (between operating points A/B)
2) relative wave directions vary for the same ship speed (between operating points C/D)
3) significant wave height and wind speed vary for similar relative wave directions and ship speeds (between operating points E/F)

The columns Δ in Table 3 present the changes between the operating points.

In case 1 (operating points A and B), where wind and wave conditions remain unchanged, the power demand depends on ship speed. Case 2, covering operating points C and D, highlights the critical role of relative wave direction: At identical ship speeds, when relative wind and wave directions shift from near-head seas (point C: 352°) to near-following seas (point D: 175°), the resulting change affects added

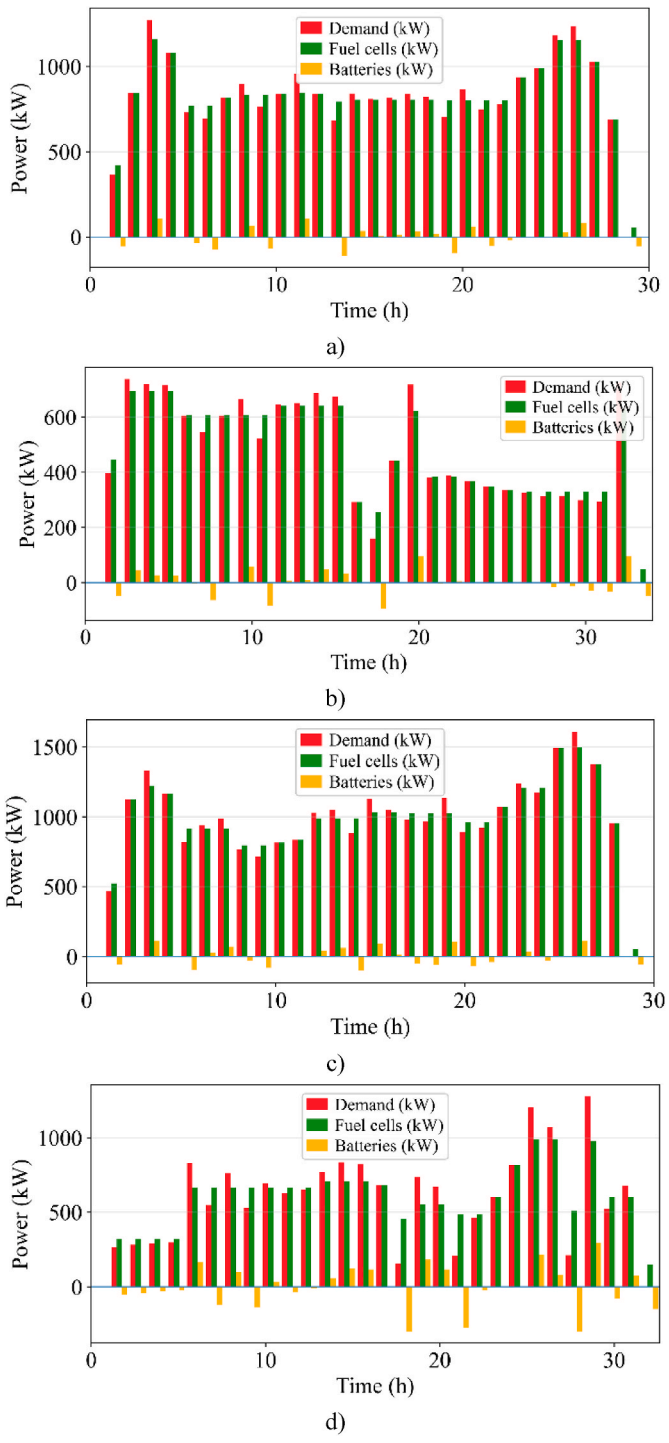

Fig. 8. Vessel power profiles for different weather conditions: a) Average-power, b) Low-power, c) High-power, d) Fluctuating (short-period high peak).

resistance and thus power demand. This effect is particularly pronounced in higher sea states, where added resistance becomes dominant. Case 3, for operating points E and F, illustrates the influence of environmental severity: even at identical ship speeds and similar relative directions, power demand differs substantially due to higher significant wave height and stronger winds at point E.

The operating points in Table 3 are illustrative examples used to examine the impact of ship speed, relative wave direction, and sea severity on power demand. The magnitude of power changes depends on the specific speeds and sea states.

4.2.3. *Lifetime cost optimization for the selected design*

The probability distribution of the NPV of total lifetime costs, for the selected configuration (15 × 100 kW fuel cells and 3x60 kWh batteries), across all voyage profiles is shown in Fig. 9. The distribution has a mean NPV of $14.9 million (with a baseline fuel price of 6$/kg), and the 5th-95th percentile range spans from $13.4-$16.6 million ($3.2 million spread), corresponding to approximately −10.3% and +11.1% deviations relative to the mean, respectively. This highlights the significant influence of weather variability on the total lifetime cost. Fuel costs account for 76% of total lifetime cost while fuel cell and battery CAPEX (including replacement costs) account for 24%. Within this capital-related share, fuel cell replacement contributes approximately 12.8% of total lifetime cost, while battery-related costs (initial investment and replacement) represent approximately 1% under the baseline scenario. This indicates that degradation-related costs have a limited influence on total lifetime cost compared to fuel expenditure.

If the installed fuel-cell capacity is increased from 1500 to 1600 kW (1 additional fuel cell module), the mean lifetime cost rises by 1.2%, due to the 6.4% total CAPEX increase (including replacements), which outweighs the 0.4% fuel cost reduction that results from a more fuel-efficient part-load operation. Similarly, if the installed battery capacity is increased from 180 to 240 kWh (1 additional battery pack), the mean lifetime cost rises by 0.4%, with a 1.3% total CAPEX increase. Hence, further capacity increases do not provide an economic advantage.

Given the fuel price dominance (76% of total cost), future changes in green hydrogen prices will have a major influence on total lifetime cost. Hydrogen prices and usage remain uncertain due to several external factors, such as electricity prices and renewable energy availability. The hydrogen price variations examined below are evaluated for the selected configuration, without re-optimizing system capacities for each price scenario.

A reduction in fuel price from 6$/kg to 3$/kg, in case of large large-scale green-hydrogen deployment, would lower the mean NPV and narrow the lifetime cost distribution spread since fuel expenses are the largest share of total lifetime cost. A lifetime cost distribution for a green hydrogen price of 3$/kg (50% reduction), based on PwC predictions (PwC, 2025), is shown in Fig. 10. The mean NPV is $9.26 million and the 5th-95th percentile range spans from $8.5 to $10.1 million ($1.6 million spread), which correspond to −8.21% and +9.07% deviations relative to the mean NPV respectively.

Conversely, a fuel price increase from 6$/kg to 9$/kg, in case of limited hydrogen availability, would widen the distribution spread as shown in Fig. 11, with a mean NPV of $20.6 million and a 5th-95th percentile range spanning from $18.3 to $23.1 million ($4.8 million spread), corresponding to −11.1% and 12.1% deviations relative to the mean NPV.

Another uncertain parameter is the number of lifetime voyages. If the vessel completes 5 fewer round trips per year, due to the speed reductions or potential port delays, the total lifetime cost is reduced by 4.8%, but the total income may also be reduced due to the lower voyage frequency. Due to the high unpredictability and the lack of reliable income data, the estimation of revenues is out of scope in this study.

The SCIP solver reported an optimality gap of 0% for all simulations, confirming that the optimization model consistently achieved globally optimal solutions (Bestuzheva et al., 2023).

5. Conclusions

This study presents a holistic MINLP framework for ship energy system design and NPV-based lifetime cost optimization, incorporating weather-driven speed profile variability and navigation safety constraints. The analysis demonstrates how weather variability affects power profiles, required energy system capacities, and total lifetime cost. While the framework is applicable to various ship types and propulsion systems, it is particularly valuable for hydrogen-powered vessels, due to the high fuel price, system costs and sensitivity to load

Table 3
Illustrative cases of speed-weather interaction on power demand (columns show paired comparison of operating points).

Variable	Operating points								
	A	B	Δ	C	D	Δ	E	F	Δ
Ship speed (knots)	11.6	9.3	*−20%*	9.7	9.7	a	9.1	9.1	a
Wave height (m)	1.3	1.3	a	0.42	0.35	a	1.71	0.24	*−86%*
Wind speed (m/s)	9.2	9.1	a	4.34	4.63	a	9.56	4.46	*−53%*
Rel. wave dir. (°)	235	247	a	352	175	*177 °*	13.3	2.9	a
Rel. wind dir. (°)	250	254	a	340	191	*149 °*	15.9	7.4	a
Results									
Added Resist. (kN)	0	0	-	7.9	0	*−100%*	42.7	5.3	*−87%*
Calm Resist. (kN)	119	71	*−41%*	81.3	81.3	*0%*	65	65	*0%*
Power (kW)	1303	608	*−53%*	810	740	*−8.7%*	895	590	*−34%*

[a]the specific values do not affect the power changes between the pairs of operating points.

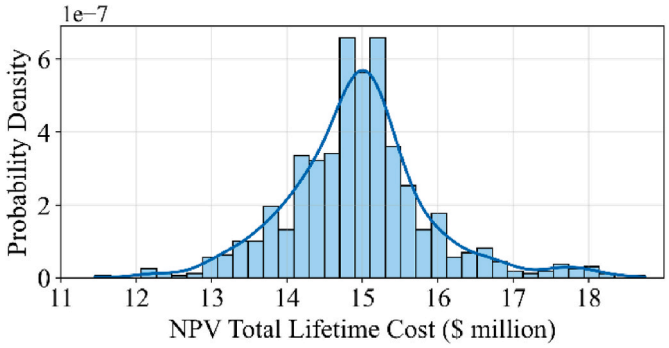

Fig. 9. Histogram of total lifetime cost (baseline fuel price: 6$/kg).

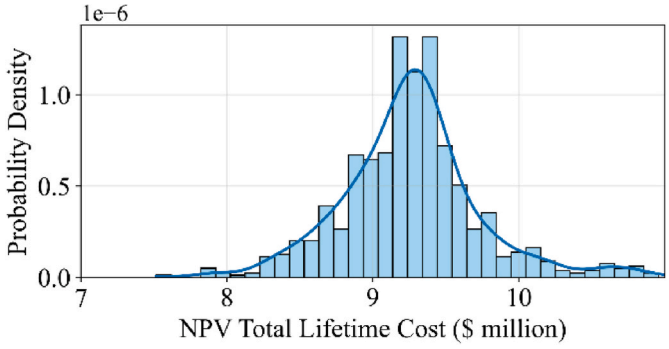

Fig. 10. Lifetime cost distribution for a fuel price of 3$/kg.

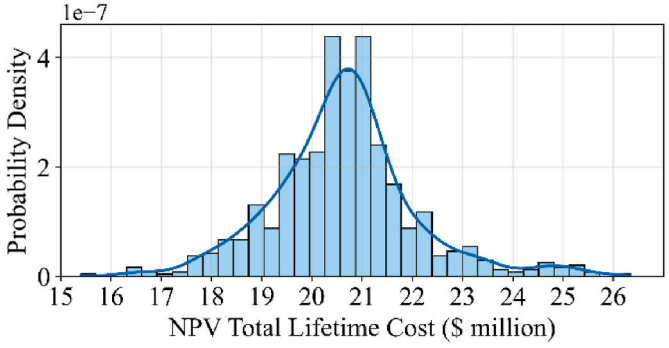

Fig. 11. Lifetime cost distribution for a fuel price of 9$/kg.

variability.

The following key results can be summarized.

- The total risk in the dataset decreases substantially from 25.25% to 6.38% (of total operating points) after applying safety-based speed reductions to mitigate resonance and successive high-wave impacts. Residual risks remain for rare scenarios (e.g., resonance at near-beam sea conditions), but these are considered operationally manageable for the case vessel, since they do not coincide with the critical sea states identified for this vessel (short wave periods of 4-8 s combined with significant wave heights exceeding 4 m).
- The combined influence of varying ship speed and weather conditions can significantly alter the vessel's power demand, requiring fuel cell capacities between 700 and 1500 kW, depending on the power profile.
- The most frequent configuration across operating profiles is a 1200 kW fuel cell system with a 180-kWh battery system (for peak shaving), covering 39% of laden profiles. Some profiles require higher fuel cell capacity for sustained peaks and/or higher battery capacity to buffer fluctuations. The selected design configuration consists of 1500 kW installed fuel cell capacity and 180 kWh battery capacity. Further system capacity increases are not cost-effective.
- The optimization across operating profiles for the selected design configuration and a baseline fuel price of 6$/kg results to a lifetime cost distribution with a 5th −95th percentile range of −10.3% to +11.1% around the mean NPV (14.9 $ million), highlighting the impact of operational and environmental variability. Fuel price reductions, in case of large-scale green hydrogen deployment and increased market adoption, would narrow this cost spread since fuel expenses are the largest share (76%) of the total lifetime cost.

Future extensions of this framework can include coupled speed-routing optimization, and enhanced hydrodynamic modelling through more advanced added wave resistance formulations. From a techno-economic perspective, the framework could be extended to include price-dependent re-optimization of system capacities under alternative hydrogen cost scenarios, and higher resolution transient operating profiles to assess short-duration power spikes, battery dispatch dynamics, degradation-aware replacement strategies, and validation against in-service power measurements.

CRediT authorship contribution statement

Foivos Mylonopoulos: Writing – review & editing, Writing – original draft, Validation, Software, Methodology, Formal analysis, Conceptualization. **Andrea Coraddu:** Writing – review & editing, Visualization, Supervision, Methodology, Funding acquisition, Conceptualization. **Henk Polinder:** Writing – review & editing, Visualization, Supervision, Methodology, Funding acquisition, Conceptualization. **Andrea Orlandi:** Conceptualization, Methodology, Writing – review &

editing.

Declaration of competing interest

The authors declare that they have no known competing financial interests or personal relationships that could have appeared to influence the work reported in this paper.

Acknowledgments

This research was supported by the Sustainable Hydrogen Integrated Propulsion Drives (SH2IPDRIVE) project, which has received funding from RVO (reference number MOB21013) through the RDM regulation of the Ministry of Economic Affairs and Climate Policy.

References

Aijjou, A., Bahatti, L., Raihani, A., 2020. Wind energy for shipboard electric power needs. Int. J. Adv. Trends Comput. Sci. Eng. 9 (1.5), 168–177. https://doi.org/10.30534/ijatcse/2020/2491.52020.

Balcombe, P., Brierley, J., Lewis, C., Skatvedt, L., Speirs, J., Hawkes, A., Staffell, I., 2019. How to decarbonise international shipping: options for fuels, technologies and policies. Energy Convers. Manag. 182, 72–88. https://doi.org/10.1016/j.enconman.2018.12.080.

Banaei, M., Ghanami, F., Khooban, M.H., Boudjadar, J., 2021. Cost-effective control of roll-on/roll-off emission-free ships. In: Proceedings of the 25th International Conference on Methods and Models in Automation and Robotics (MMAR). https://doi.org/10.1109/MMAR49549.2021.9528473.

Bassam, A.M., Phillips, A.B., Turnock, S.R., Wilson, P.A., 2016a. An improved energy management strategy for a hybrid fuel cell/battery passenger vessel. Int. J. Hydrogen Energy 41 (47), 22453–22464. https://doi.org/10.1016/j.ijhydene.2016.08.049.

Bassam, A.M., Phillips, A.B., Turnock, S.R., Wilson, P.A., 2016b. Sizing optimization of a fuel cell/battery hybrid system for a domestic ferry using a whole ship system simulator. In: International Conference on Electrical Systems for Aircraft, Railway, Ship Propulsion and Road Vehicles and International Transportation Electrification Conference. ESARS-ITEC). https://doi.org/10.1109/ESARS-ITEC.2016.7841333, 2016.

Bassam, A.M., Phillips, A.B., Turnock, S.R., Wilson, P.A., 2017. Development of a multi-scheme energy management strategy for a hybrid fuel cell driven passenger ship. Int. J. Hydrogen Energy 42 (1), 623–635. https://doi.org/10.1016/j.ijhydene.2016.08.209.

Bestuzheva, K., Chmiela, A., Müller, B., Serrano, F., Vigerske, S., Wegscheider, F., 2023. Global optimization of mixed-integer nonlinear programs with SCIP 8. J. Global Optim. 91, 287–310. https://doi.org/10.1007/s10898-023-01345-1.

Copernicus Climate Change Service, 2018. ERA5 hourly data on single levels from 1940 to present. https://doi.org/10.24381/cds.adbb2d47. (Accessed 15 May 2025).

Coraddu, A., Figari, M., Savio, S., 2014. Numerical investigation on ship energy efficiency by monte carlo simulation. Proc. Inst. Mech. Eng. M J. Eng. Marit. Environ. 228 (3), 220–234. https://doi.org/10.1177/1475090214524184.

Dall'Armi, C., Pivetta, D., Taccani, R., 2021. Health-conscious optimization of long-term operation for hybrid PEMFC ship propulsion systems. Energies 14 (13), 3813. https://doi.org/10.3390/en14133813.

Dall'Armi, C., Pivetta, D., Taccani, R., 2022. Uncertainty analysis of the optimal health-conscious operation of a hybrid PEMFC coastal ferry. Int. J. Hydrogen Energy 47 (21), 11428–11440. https://doi.org/10.1016/j.ijhydene.2021.10.271.

De Gracia, L., Osawa, N., Tamaru, H., Fukasawa, T., 2018. A comparative study on fatigue damage using a wave load sequence model. KnE Eng 3 (1), 160–170. https://doi.org/10.18502/keg.v3i1.1422.

Degiuli, N., Martić, I., Farkas, A., Gospić, I., 2021. The impact of slow steaming on reducing CO_2 emissions in the Mediterranean Sea. Energy Rep. 7, 8131–8141. https://doi.org/10.1016/j.egyr.2021.02.046.

Degiuli, N., Martić, I., Grlj, C.G., 2024. Slow steaming as a sustainable measure for low-carbon maritime transport. Sustainability 16 (24), 11169. https://doi.org/10.3390/su162411169.

Esmailian, E., Steen, S., Koushan, K., 2022. Ship design for real sea states under uncertainty. Ocean. Eng. 266, 113127. https://doi.org/10.1016/j.oceaneng.2022.113127.

Fabbri, T., Vicen-Bueno, R., 2019. Weather-routing system based on METOC navigation risk assessment. J. Mar. Sci. Eng. 7 (5), 127. https://doi.org/10.3390/jmse7050127.

Fan, A., Yan, X., Bucknall, R., Yin, Q., Ji, S., Liu, Y., Song, R., Chen, X., 2020. A novel ship energy efficiency model considering random environmental parameters. J. Mar. Eng. Technol. 19 (4), 215–228. https://doi.org/10.1080/20464177.2018.1546644.

Farkas, A., Degiuli, N., Martić, I., Grlj, C.G., 2022. Is slow steaming a viable option to meet the novel energy efficiency requirements for containerships? J. Clean. Prod. 374, 133915. https://doi.org/10.1016/j.jclepro.2022.133915.

Gritsenko, D., 2017. Regulating GHG emissions from shipping: local, global, or polycentric approach? Mar. Pol. 84, 130–133. https://doi.org/10.1016/j.marpol.2017.07.010.

Han, J., Charpentier, J.F., Tang, T., 2014. An energy management system of a fuel cell/battery hybrid boat. Energies 7 (5), 2799–2820. https://doi.org/10.3390/en7052799.

International Maritime Organization (IMO), 2007. Revised Guidance to the Master for Avoiding Dangerous Situations in Adverse Weather and Sea Conditions. IMO, London. https://wwwcdn.imo.org/localresources/en/OurWork/Safety/Documents/Stability/MSC.1-CIRC.1228.pdf.

International Maritime Organization (IMO), 2021. Guidelines for Determining Minimum Propulsion Power to Maintain the Manoeuvrability of Ships in Adverse Conditions (MEPC.1/Circ.850/Rev.3). IMO, London. https://www.classnk.or.jp/hp/pdf/activities/statutory/eedi/13_MEPC.1-CIRC.850-Rev.3.pdf.

International Maritime Organization (IMO), 2023. 2023 IMO strategy on reduction of GHG emissions from ships. https://www.imo.org/en/ourwork/environment/pages/2023-imo-strategy-on-reduction-of-ghg-emissions-from-ships.aspx. (Accessed 20 October 2025).

International Towing Tank Conference (ITTC), 2005. ITTC Recommended Procedures and Guidelines: Analysis of Speed/Power Trial Data, Procedure 7.5-04-01-01.2. ITTC. Nantes, France. https://ittc.info/media/1363/75-04-01-012.pdf.

ISO, 2015. ISO 15016:2015 – Ships and Marine Technology: Guidelines for the Assessment of Speed and Power Performance by Analysis of Speed Trial Data. ISO, Geneva, Switzerland.

Khan, L., Macklin, J.J.R., Peck, B.C.D., Morton, O., Souppez, J.-B.R.G., 2021. A review of wind-assisted ship propulsion for sustainable commercial shipping: latest developments and future stakes. In: Wind Propulsion Conference. https://doi.org/10.3940/rina.win.2021.05, 15–16 September 2021, London, UK.

Kim, Y.R., Esmailian, E., Steen, S., 2022. A meta-model for added resistance in waves. Ocean. Eng. 266, 112749. https://doi.org/10.1016/j.oceaneng.2022.112749.

Krata, P., Wawrzyński, W., 2016. Prediction of the natural frequency of ship's roll with regard to various models of roll damping. J. KONES Powertrain Transp. 23 (3), 289–296. https://doi.org/10.5604/12314005.1216499.

Kytariolou, A., Themelis, N., 2022. Ship routing optimisation based on forecasted weather data and considering safety criteria. J. Navig. 75 (6), 1310–1331. https://doi.org/10.1017/S0373463322000613.

Lagemann, B., Lagouvardou, S., Lindstad, E., Fagerholt, K., Psaraftis, H.N., Erikstad, S.O., 2023. Optimal ship lifetime fuel and power system selection under uncertainty. Transp. Res. D. 119, 103748. https://doi.org/10.1016/j.trd.2023.103748.

Lang, X., Mao, W., 2021. A practical speed loss prediction model at arbitrary wave heading for ship voyage optimization. J. Mar. Sci. Appl. 20, 410–425. https://doi.org/10.1007/s11804-021-00224-z.

Liu, X., Yan, Z., Wu, J., 2019. Optimal coordinated operation of a multi-energy community considering interactions between energy storage and conversion devices. Appl. Energy 248, 256–273. https://doi.org/10.1016/j.apenergy.2019.04.106.

Mittendorf, M., Nielsen, U.D., Bingham, H.B., Liu, S., 2022. Towards the uncertainty quantification of semi-empirical formulas applied to the added resistance of ships in waves of arbitrary heading. Ocean. Eng. 251, 111040. https://doi.org/10.1016/j.oceaneng.2022.111040.

Mylonopoulos, F., Durgaprasad, S., Coraddu, A., Polinder, H., 2024. Lifetime design, operation, and cost analysis for the energy system of a retrofitted cargo vessel with fuel cells and batteries. Int. J. Hydrogen Energy 91, 1262–1273. https://doi.org/10.1016/j.ijhydene.2024.10.235.

Mylonopoulos, F., Coraddu, A., Polinder, H., 2026. A holistic framework for optimal ship energy system design, including operational requirements, lifetime cost, and vessel stability. Energy Convers. Manag. X. 30, 101685. https://doi.org/10.1016/j.ecmx.2026.101685.

Papanikolaou, A., 2014. Ship Design: Methodologies of Preliminary Design. Springer, Dordrecht. https://doi.org/10.1007/978-94-017-8751-2.

Park, D.M., Lee, J.H., Jung, Y.W., Lee, J., Kim, Y., Gerhardt, F., 2019. Experimental and numerical studies on added resistance of ship in oblique sea conditions. Ocean. Eng. 186, 106070. https://doi.org/10.1016/j.oceaneng.2019.05.052.

Pelić, V., Bukovac, O., Radonja, R., Degiuli, N., 2023. The impact of slow steaming on fuel consumption and CO_2 emissions of a container ship. J. Mar. Sci. Eng. 11 (3), 675. https://doi.org/10.3390/jmse11030675.

Pennino, S., Gaglione, S., Innac, A., Piscopo, V., Scamardella, A., 2020. Development of a new ship adaptive weather routing model based on seakeeping analysis and optimization. J. Mar. Sci. Eng. 8 (4), 270. https://doi.org/10.3390/jmse8040270.

Pericic, M., Vladimir, N., Jovanovic, I., Korican, M., 2022. Application of fuel cells with zero-carbon fuels in short-sea shipping. Appl. Energy 309, 118463. https://doi.org/10.1016/j.apenergy.2021.118463.

Pivetta, D., Dall'Armi, C., Taccani, R., 2021. Multi-objective optimization of hybrid PEMFC/Li-ion battery propulsion systems for small and medium size ferries. Int. J. Hydrogen Energy 46 (72), 35949–35960. https://doi.org/10.1016/j.ijhydene.2021.02.124.

PowerCell Sweden, A.B., 2019. PowerCell to Present New Version of MS-100 Fuel Cell System for Electrification on Land and at Sea. Press release, 4 November 2019. https://powercellgroup.com/press-releases/powercell-to-present-new-version-of-ms-100-fuel-cell-system-for-electrification-on-land-and-at-sea/. (Accessed 1 March 2024).

Praxis Automation Technology B.V., 2024. GreenBattery. https://www.praxis-automation.eu/products/electricenergy-storage/. (Accessed 1 March 2024).

PwC, 2025. The green hydrogen economy – predicting the decarbonisation agenda of tomorrow. https://www.pwc.com/gx/en/industries/energy-utilities-resources/green-hydrogen-cost.html. (Accessed 23 August 2025).

Seo, D.W., Oh, J., 2021. Uncertainty analysis of speed–power performance based on measured raw data in sea trials. Int. J. Nav. Archit. Ocean Eng. 13, 396–404. https://doi.org/10.1016/j.ijnaoe.2021.04.001.

Soni, G., Neto, R.C., Moreira, L., 2023. Hydrodynamic simulation of green hydrogen catamaran operating in Lisbon, Portugal. J. Mar. Sci. Eng. 11 (12), 2273. https://doi.org/10.3390/jmse11122273.

Vahabzad, N., Mohammadi-Ivatloo, B., Anvari-Moghaddam, A., 2022. Modeling hybrid energy systems for marine applications: hybrid electric ships. In: Lo Faro, M., Barbera, O., Giacoppo, G. (Eds.), Hybrid Technologies for Power Generation: Hybrid Energy Systems. Academic Press, pp. 419–437. https://doi.org/10.1016/B978-0-12-823793-9.00012-7.

Vieira, G.T.T., Pereira, D.F., Taheri, S.I., Khan, K.S., Salles, M.B.C., Guerrero, J.M., Carmo, B.S., 2022. Optimized configuration of diesel engine–fuel cell–battery hybrid power systems in a platform supply vessel to reduce CO_2 emissions. Energies 15 (6), 2184. https://doi.org/10.3390/en15062184.

Wang, X., Shipurkar, U., Haseltalab, A., Polinder, H., Claeys, F., Negenborn, R.R., 2021. Sizing and control of a hybrid ship propulsion system using multi-objective double-layer optimization. IEEE Access 9, 72587–72601. https://doi.org/10.1109/ACCESS.2021.3080195.

Zhang, D., Song, Y., Gao, J., Shen, Z., Li, L., Yao, A., 2025. Research on ship engine fuel consumption prediction algorithm based on adaptive optimization generative network. J. Mar. Sci. Eng. 13 (6), 1140. https://doi.org/10.3390/jmse13061140.

Zhang, Z., Guan, C., Liu, Z., 2020. Real-time optimization energy management strategy for fuel cell hybrid ships considering power sources degradation. IEEE Access 8, 87046–87059. https://doi.org/10.1109/ACCESS.2020.2991519.

Zis, T.P.V., Psaraftis, H.N., Ding, L., 2020. Ship weather routing: a taxonomy and survey. Ocean. Eng. 213, 107697. https://doi.org/10.1016/j.oceaneng.2020.107697.